



Urban aerosol chemistry at a land-water transition site during summer – Part 2: Aerosol pH and liquid water content

Michael A. Battaglia, Jr.^{1,a}, Nicholas Balasus¹, Katherine Ball¹, Vanessa Caicedo², Ruben
Delgado², Annmarie G. Carlton³, and Christopher J. Hennigan^{1*}

¹Department of Chemical, Biochemical, and Environmental Engineering, University of Maryland, Baltimore County

²Joint Center for Earth Systems Technology, University of Maryland, Baltimore County

³Department of Chemistry, University of California, Irvine

^aCurrent affiliation: School of Earth and Atmospheric Sciences, Georgia Institute of Technology

Correspondence: C. J. Hennigan (hennigan@umbc.edu)

1 **Abstract**

2

3

4

5

6

7

8

9

10

11

12

13

Particle acidity (aerosol pH) is an important driver of atmospheric chemical processes and the resulting effects on human and environmental health. Understanding the factors that control aerosol pH is critical when enacting control strategies targeting specific outcomes. This study characterizes aerosol pH at a land-water transition site near Baltimore, MD during summer 2018 as part of the second Ozone Water-Land Environmental Transition Study (OWLETS-2) field campaign. Inorganic fine mode aerosol composition, gas-phase NH₃ measurements, and all relevant meteorological parameters were used to characterize the effects of temperature, aerosol liquid water (ALW), and composition on predictions of aerosol pH. Temperature, the factor linked to the control of NH₃ partitioning, was found to have the most significant effect on aerosol pH during OWLETS-2. Overall, pH varied with temperature at a rate of -0.047 K⁻¹ across all observations, though the sensitivity was -0.085 K⁻¹ for temperatures > 293 K. ALW had a minor



14 effect on pH, except at the lowest ALW levels ($< 1 \mu\text{g m}^{-3}$) which caused a significant increase
15 in aerosol acidity (decrease in pH). Aerosol pH was generally insensitive to composition (SO_4^{2-} ,
16 $\text{SO}_4^{2-}:\text{NH}_4^+$, $\text{Tot-NH}_3 = \text{NH}_3 + \text{NH}_4^+$), consistent with recent studies in other locations. In a
17 companion paper, the sources of episodic NH_3 events (95th percentile concentrations, $\text{NH}_3 > 7.96$
18 $\mu\text{g m}^{-3}$) during the study are analyzed; aerosol pH was higher by only ~ 0.1 - 0.2 pH units during
19 these events compared to the study mean. A case study was analyzed to characterize the
20 response of aerosol pH to nonvolatile cations (NVCs) during a period strongly influenced by
21 primary Chesapeake Bay emissions. Depending on the method used, aerosol pH was estimated
22 to be either weakly (~ 0.1 pH unit change based on NH_3 partitioning calculation) or strongly
23 (~ 1.4 pH unit change based on ISORROPIA thermodynamic model predictions) affected by
24 NVCs. The case study suggests a strong pH gradient with size during the event and underscores
25 the need to evaluate assumptions of aerosol mixing state applied to pH calculations. Unique
26 features of this study, including the urban land-water transition site and the strong influence of
27 NH_3 emissions from both agricultural and industrial sources, add to the understanding of aerosol
28 pH and its controlling factors in diverse environments.



29 **1 Introduction**

30

31 The acidity, or pH, of atmospheric aerosols affects the chemical and physical properties
32 of airborne particles, and thus, their impacts on climate and health (Pye et al., 2020). The gas-
33 particle partitioning of semi-volatile acidic and basic compounds – notably NH_3 , HNO_3 , HCl ,
34 and organic acids – depends in part on aerosol pH, which directly affects the particulate matter
35 (PM) mass concentration (Nenes et al., 2020). The solubility of many particulate components is
36 pH-dependent, including metals and nutrients, with implications for particle toxicity and nutrient
37 deposition to ecosystems (Fang et al., 2017; Kanakidou et al., 2016). The optical properties of
38 light-absorbing organic compounds, known as brown carbon, can exhibit a strong pH-
39 dependence, which directly affects their climate impacts (Phillips et al., 2017). Given the
40 importance of aerosol pH for atmospheric processes and the limitation in estimating acidity with
41 proxies (e.g., ion balances), there has been increased effort in recent years to identify the factors
42 that affect pH and to characterize temporal and spatial variations in the atmosphere (Hennigan et
43 al., 2015).

44 Globally, aerosol pH is often quite acidic due to the ubiquity and abundance of strong
45 acids like H_2SO_4 , HNO_3 , and HCl (Pye et al., 2020). Ammonia (NH_3) is unique among species
46 that affect pH because it is the most abundant basic compound in the atmosphere. NH_3
47 partitioning is controlled by the concentration of strong acids and by the ambient temperature
48 and relative humidity, hence, the dependence of pH on both composition and meteorology
49 (Zheng et al., 2020). This explains why NH_3 can exist partially in the gas phase even when the
50 aerosol pH is highly acidic (Weber et al., 2016). Due to its abundance and semi-volatile
51 properties, NH_3 was identified as the most important buffering agent in aerosols across locations
52 with diverse emissions, composition, and climatology (Zheng et al., 2020). In single-phase



53 aqueous particles, organic compounds have a minor effect on pH (Battaglia Jr et al., 2019),
54 though this is not the case for particles that have undergone liquid-liquid phase separation (Pye et
55 al., 2018). Non-volatile cations (NVC) typically contribute a minor fraction of PM mass but can
56 be critical for accurate predictions of pH, especially if NVC concentrations are overestimated
57 (Vasilakos et al., 2018). Globally, NVC are most important in regions heavily impacted by dust
58 emissions (Pye et al., 2020), but have minor effects on pH in other regions (Tao and Murphy,
59 2019; Zheng et al., 2020).

60 Aerosol pH is also strongly affected by meteorological factors. Equilibrium constants,
61 including those that determine the gas-particle partitioning and aqueous dissociation of semi-
62 volatile acids and bases, are temperature dependent. Temperature is a dominant factor driving
63 variability in the seasonal and diurnal cycling of pH (Guo et al., 2015; Tao and Murphy, 2019).
64 Temperature gradients, as occur in and around urban areas, can also drive large differences in
65 pH, even if the composition is uniform over the same scales (Battaglia et al., 2017). Relative
66 humidity (RH) regulates aerosol liquid water content (ALWC), which affects the partitioning of
67 soluble gases and aqueous phase solute concentrations. ALWC may be the most important
68 factor responsible for large pH differences observed between the southeast US (pH ~0.5-1.0) and
69 the heavily polluted North China Plain (pH ~4-5), the two regions where pH has been most
70 extensively studied to-date (Zheng et al., 2020). These effects can be complex, or even partially
71 offset. For example, an increase in temperature reduces pH owing to the shift in NH_3
72 partitioning towards the gas phase, but NH_3 emissions increase with temperature as well,
73 producing an increase in pH and partially offsetting the pH changes due to temperature (Tao,
74 2020). More research is needed to better understand how all these factors together affect pH, and
75 how this changes geographically and temporally.



76 In this study aerosol pH was characterized during the summertime (June 4 to July 5,
77 2018) at a land-water transition site near a large urban area (Baltimore, MD) as part of the
78 OWLETS-2 (second Ozone Water-Land Environmental Transition Study) field campaign. This
79 site is unique because meteorological phenomena, such as the bay breeze, affect pollution
80 dispersion and recirculation (Loughner et al., 2014). Baltimore is impacted by different regional
81 emission sources, as it is located in the populous and heavily trafficked I-95 corridor, and
82 downwind of the Ohio River Valley (He et al., 2013), and relatively close to regional agricultural
83 operations that emit large amounts of NH_3 (Pinder et al., 2006). In the companion investigation,
84 the local sources of NH_3 during the OWLETS-2 study were examined, including an analysis of
85 transient events with unexpectedly high NH_3 concentrations (Balasus et al., 2021). In this study,
86 the effects of the observed NH_3 concentrations (including transient concentrations of
87 unexpectedly high values), in combination with the unique meteorological phenomena associated
88 with the land-water transition, on ALW and aerosol pH were investigated.

89

90 **2 Methods**

91 The OWLETS-2 study was conducted to characterize effects of meteorological
92 phenomena associated with the land-water transition on summertime air quality in Baltimore.
93 Hart-Miller Island (HMI, coordinates 39.2421° , -76.3627°), a site located on the Chesapeake Bay
94 ~10 km east of downtown Baltimore, hosted many of the ground-based measurements during the
95 study (Fig. S1). Semi-continuous measurements of aerosol inorganic chemical composition and
96 gas-phase NH_3 were conducted at HMI. The measurement details are provided in the companion
97 paper (Balasus et al., 2021). Briefly, the water-soluble ionic components of $\text{PM}_{2.5}$ were
98 measured with a Particle-into-Liquid Sampler coupled to a dual Ion Chromatograph (PILS-IC,



99 Metrohm) operated according to Valerino et al. (2017). NH_3 was measured with an AiRRmonia
100 Analyzer (RR Mechatronics) (Norman et al., 2009). Meteorological parameters were measured
101 with a Vaisala MAWS201 Met Station at 1-minute resolution.

102 The 5-minute NH_3 measurements and 1-minute meteorological measurements were
103 averaged to the 20-minute sampling time of the PILS-IC. Aerosol pH for each 20-min sample
104 was calculated according to Zheng et al. (2020). This method uses the relevant temperature-
105 dependent equilibrium constants and the measured concentrations of NH_3 and $[\text{NH}_4^+]$ to
106 calculate pH. The method of Zheng et al. (2020) is based upon a similar approach in prior
107 studies (Hennigan et al., 2015; Keene et al., 2004), with minor differences possibly due to
108 equilibrium constant values and/or the concentration basis (molality vs. molarity). Indeed, very
109 close agreement was observed (slope = 0.967, $R^2 = 0.977$, $n = 872$, Fig. S2) in calculated pH
110 between the methods of Zheng et al. (2020) and Hennigan et al. (2015). The aqueous phase
111 NH_4^+ concentration is derived from the mass concentration of NH_4^+ from the PILS-IC and the
112 ALWC. The ISORROPIA-II thermodynamic equilibrium model was used to calculate ALW
113 using the PILS-IC, NH_3 , and meteorological data as inputs (Fountoukis and Nenes, 2007). The
114 model was run in forward mode (NH_3 and aerosol NH_4^+ were input at total NH_3) using the
115 metastable assumption according to the recommendation of Guo et al. (2015).

116 Although ISORROPIA can provide pH, the methods of Zheng et al. (2020) and Tao et al.
117 (2020) were used for pH calculations:

$$118 \quad \text{pH} = \text{p}K_{a,\text{NH}_3}^* + \log_{10} \frac{[\text{NH}_3(\text{aq})] + [\text{NH}_3(\text{g})]}{[\text{NH}_4^+(\text{aq})]} \quad (1)$$

$$119 \quad [\text{NH}_3(\text{g})] = \frac{p_{\text{NH}_3} \rho_w}{RT \text{ AWC}} \quad (2)$$

$$120 \quad K_{a,\text{NH}_3}^* = \frac{[\text{H}^+(\text{aq})]([\text{NH}_3(\text{aq})] + [\text{NH}_3(\text{g})])}{[\text{NH}_4^+(\text{aq})]} = K_{a,\text{NH}_3} \left(1 + \frac{\rho_w}{H_{\text{NH}_3} RT \text{ AWC}} \right) \quad (3)$$



121 where in Equation 1, $[NH_3(aq)]$ is the molality of NH_3 in solution (mol kg^{-1} , calculated by
122 multiplying H_{NH_3} and p_{NH_3}), $[NH_3(g)]$ is the equivalent molality of gaseous NH_3 in solution
123 (mol kg^{-1} , given by Equation 2), and $[NH_4^+(aq)]$ is the molality of NH_4^+ in solution (mol kg^{-1}).
124 Equation 2 calculates $[NH_3(g)]$, where p_{NH_3} is the partial pressure of NH_3 (atm), ρ_w is the
125 density of water ($\mu\text{g m}^{-3}$), R is the gas constant ($\text{atm L mol}^{-1} \text{K}^{-1}$), T is temperature (K), and
126 AWC is aerosol water content ($\mu\text{g m}^{-3}$ air). Equation 3 calculates the last unknown term in
127 Equation 1, which is K_{a,NH_3}^* , the effective dissociation constant (where H_{NH_3} is the Henry's law
128 constant of NH_3 in $\text{mol kg}^{-1} \text{atm}^{-1}$).

129 Direct measurements of aerosol pH are not available to test model predictions so the
130 partitioning of semi-volatile species that depend on pH, most commonly NH_3/NH_4^+ and
131 HNO_3/NO_3^- , is a key metric used to evaluate model performance (Pye et al., 2020).
132 ISORROPIA is used extensively for predictions of pH; however, in this study the measured and
133 ISORROPIA-predicted values of NH_3 partitioning ($\epsilon_{NH_3} = NH_3/(NH_3 + NH_4^+)$) did not agree well
134 (Fig. S3). There were systematic differences in pH between the two methods (mean pH
135 difference = 0.6 pH units), and they were not correlated ($R^2 = 0.097$, not shown). The source of
136 the discrepancy in NH_3 partitioning (ISORROPIA modeled versus measurement-calculated) is
137 unknown, though it is not likely the result of an incorrect assumption of equilibrium (see the SI
138 and the companion paper Balasus et al. (2021) for more details).

139

140 **3 Results and Discussion**

141 **3.1 Meteorological effect on pH**

142 As in many cities, the urban heat island effect in Baltimore evolves throughout the day,
143 with urban-rural temperature and RH gradients peaking at night (Battaglia et al., 2017).



144 Meteorological conditions at HMI demonstrate unique features associated with the land-water
145 transition. At night, the average temperature observed at HMI was close to conditions observed
146 in downtown Baltimore but transitioned to match the conditions at a nearby rural site during the
147 day (Fig. 1a). Overall, the range in average hourly temperatures at HMI was lower (4.3 °C; 22.5
148 – 26.8 °C) than the averages observed at either the downtown site (range 6.2 °C; 22.8 – 29.0 °C)
149 or the rural site (range 8.8 °C; 17.5 – 26.3 °C). Likewise, the average hourly RH profile at HMI
150 had a significantly smaller range (13.7%; 61.7 – 75.4%) than the RH profiles at the downtown
151 (range 22.1%; 53.2 – 75.3%) or rural sites (range 30.3%; 55.9 – 86.2%) (Fig. 1b). The
152 differences shown in Fig. 1 were due to the proximity of HMI to the Chesapeake Bay. This has
153 strong implications for aerosol pH, which will be discussed in detail below.

154 Due to the meteorological conditions discussed above, the diurnal profile of ALWC at
155 HMI was unique (Fig. 2a). Typical profiles of ALWC in the eastern US closely follow RH, with
156 minima in the afternoon and maxima at night or in the pre-dawn morning hours (Guo et al.,
157 2015; Battaglia et al., 2017). During OWLETS-2, ALWC did not show a distinct diurnal profile
158 that was correlated with RH. Instead, the highest median ALWC at HMI occurred between
159 12:00 – 14:00, (local time, LT; during the study this is UTC-4) (Fig. 2a). This daily peak in
160 ALWC coincided with a pronounced enhancement in aerosol NO_3^- , which is discussed in the
161 companion paper (Balasus et al., 2021). The partitioning of NH_3 , ϵ_{NH_3} , also showed a diurnal
162 profile that was unexpected (Fig. 2b). Due to the strong temperature dependence of vapor
163 pressure and equilibrium constants, NH_3 partitioning typically shifts towards the gas-phase
164 during the daytime (ϵ_{NH_3} increases) and shifts towards the aerosol phase at night (ϵ_{NH_3} decreases)
165 (Guo et al., 2017). The increase in gas-phase NH_3 emissions with increasing temperature can
166 also contribute to an elevated ϵ_{NH_3} during the daytime. The diurnal profile of ϵ_{NH_3} observed at



167 HMI did not follow temperature, as the median $\varepsilon_{\text{NH}_3}$ peaked during the 06:00 – 08:00 LT, and
168 decreased slightly into the afternoon (Fig. 2b). This shows a shift of NH_3 partitioning towards
169 the condensed phase as daily temperatures peaked. This was allowed by the ALWC remaining
170 steady throughout the afternoon. Overall, the median $\varepsilon_{\text{NH}_3}$ value for the entire OWLETS-2 study
171 was 0.915, showing NH_3 partitioning was shifted towards the gas-phase.

172 The diurnal profile of aerosol pH computed using the method of Zheng et al. (2020)
173 followed a qualitatively similar pattern to prior studies (Battaglia et al. 2017), with maxima in
174 the early morning and minima in the afternoon; however, there was a much smaller amplitude in
175 the median hourly pH values (Fig. 3). The highest median pH value (1.97) was observed
176 between 07:00 – 08:00 LT, while the lowest median pH (1.50) was observed between 16:00 –
177 17:00 LT. For the entire study, there was only a ~ 1 pH unit difference between the 10th and 90th
178 percentile values (1.39 and 2.36, respectively). The relatively muted diurnal profile of aerosol
179 pH was due to the unique meteorology that resembled a nearby urban site at night and
180 transitioned to match the nearby rural site during the day. The companion paper shows the
181 diurnal profiles of aerosol inorganic composition (Balasus et al., 2021). Figures 2 and 3 are
182 consistent with recent studies that demonstrate the high sensitivity of pH to meteorological
183 factors (Battaglia et al., 2017; Tao and Murphy, 2019; Zheng et al., 2020). It is interesting to
184 note that the ISORROPIA predictions of aerosol pH yield a distinctly different diurnal profile
185 than the pH predicted by NH_3 partitioning (Fig. S4). The difference in pH between the two
186 methods peaked in the afternoon between 12:00 – 14:00 LT, when particles were most acidic,
187 and was a minimum in the early morning when pH was highest (Fig. S4). The reason for these
188 discrepancies are explored in the discussion below.



189 Results suggest that pH was most sensitive to temperature changes at HMI during
190 OWLETS-2 (Fig. 4a). Across the full temperature range, the observed pH sensitivity to
191 temperature was -0.047 K^{-1} . A recent study contrasting pH in the southeast US and the North
192 China Plain found that temperature affects pH linearly at a rate of approximately -0.055 K^{-1}
193 (Zheng et al., 2020). A separate study from a Canadian observational network found that the
194 pH-temperature dependence is not linear, but changes with temperature (Tao and Murphy, 2019;
195 Tao, 2020). Over the range of conditions observed during OWLETS-2, Tao (2020) computed a
196 pH sensitivity to temperature of approximately -0.045 K^{-1} to -0.055 K^{-1} . In a previous study, the
197 pH sensitivity to temperature in Baltimore was -0.048 K^{-1} , though this was calculated for
198 conditions of constant atmospheric composition (Battaglia et al., 2017). While present results
199 share consistencies with these studies, the results in Fig. 4a suggest important differences, as
200 well. An increase in pH was observed with increasing temperature for conditions below 293 K
201 ($n=156$). In the companion paper, NH_3 concentrations dramatically increased with temperature <
202 293 K but exhibited a much weaker dependence on temperature for conditions > 293 K (Balasus
203 et al., 2021). Under the warmer conditions, the pH relationship with temperature was linear
204 during OWLETS-2, with a sensitivity of -0.085 K^{-1} (Fig. 4a). The results in Fig. 4a are
205 consistent with Tao (2020), as they demonstrate the offsetting responses of pH to temperature
206 through effects on NH_3 emissions and partitioning.

207 These results contribute to the growing body of work demonstrating the importance of
208 temperature to aerosol pH. Collectively, these studies suggest that the sensitivity of pH to
209 temperature is constrained between -0.045 K^{-1} and -0.085 K^{-1} , although the present results
210 illustrate circumstances where a positive relationship between temperature and pH can exist, as
211 well. It is notable that similar $\Delta\text{pH}/\Delta T$ values are observed across a range of locations and for



212 variable data sets that include monthly averages of long-term observations (Tao and Murphy,
213 2019) and 20-min measurements made over a period of weeks (presented here).

214 Aerosol pH was not strongly affected by ALWC over the range of conditions observed
215 during OWLETS-2, except at ALWC below $1 \mu\text{g m}^{-3}$ (Fig. 4b). At the lowest ALWC levels, the
216 increase in pH occurs because of the diluting effect of water, however, at ALWC above $1 \mu\text{g m}^{-3}$,
217 other factors appear to be more important (e.g., temperature). ALWC was recently identified as
218 the most significant contributor to regional pH differences (Zheng et al., 2020). In that study, the
219 pH-ALWC relationship was highly non-linear, with the greatest sensitivity calculated at ALWC
220 at levels $< 25 \mu\text{g m}^{-3}$, conditions corresponding to all the OWLETS-2 observations. Tao (2020)
221 found that pH is extremely sensitive to RH, presumed to be a surrogate for ALWC, when RH
222 was $< 20\%$ or $\text{RH} > 80\%$; however, pH was quite insensitive to RH variations in the region of
223 $20\% < \text{RH} < 80\%$. Approximately 25% (208 out of 875) of RH values during OWLETS-2 were
224 above 80%, yet no increase in pH was observed at the highest ALWC, suggesting that other
225 factors were offsetting the diluting effect of water as ALWC increased. It is interesting to note
226 that ISORROPIA predicts a stronger effect of ALWC on pH, with the diluting effect apparent as
227 pH increases with increasing ALWC (Fig. 4b).

228 The result shown in Fig. 4b is somewhat surprising because NH_3 partitioning was quite
229 sensitive to ALWC (Fig. 5); the relatively invariant aerosol pH is unexpected given the increase
230 in NH_3 uptake in the presence of ALW. NH_3 partitioning shifted towards the condensed phase
231 (ϵ_{NH_3} decreased) at increasing ALWC, consistent with the results of Nenes et al. (2020). ϵ_{NH_3}
232 was more sensitive to ALWC than it was to either temp or RH (Fig. S6). This result shows the
233 importance that ALWC can have on $\text{PM}_{2.5}$ mass concentrations, as water serves as an important
234 medium enhancing the condensation of organic and inorganic water-soluble species (Carlton et



235 al., 2018; El-Sayed et al., 2016). Fig. 5 demonstrates the importance of ALWC in changing the
236 dry deposition of reactive nitrogen species. Nenes et al. (2021) predicts that NH_3 and HNO_3 dry
237 deposition rates will both be high under the conditions observed during OWLETS-2 (i.e., ALWC
238 $< 10 \mu\text{g m}^{-3}$ and $\text{pH} \sim 1.5$). This is also consistent with a modeling study showing increased dry
239 deposition of reactive nitrogen in coastal regions, including the OWLETS-2 study domain
240 (Loughner et al., 2016).

241

242 **3.2 Composition Effects on Aerosol pH**

243 In contrast to meteorological factors, aerosol composition did not have a major effect on
244 pH variability during OWLETS-2. Consistent with prior studies, neither the sulfate
245 concentration nor the $\text{NH}_4^+:\text{SO}_4^{2-}$ molar ratio contributed significantly to pH variability (Weber
246 et al., 2016; Hennigan et al., 2015). Fig. 4c shows that pH was also relatively insensitive to the
247 Tot- NH_3 concentration, in agreement with the results from other locations (Zheng et al., 2020;
248 Tao, 2020; Weber et al., 2016). While the predictions of ISORROPIA generally did not capture
249 the trends between pH and the meteorological factors, it is interesting to note that ISORROPIA
250 predicts that pH is relatively insensitive to Tot- NH_3 , as well, except at the highest concentrations
251 (Fig. S5).

252 Composition and concentration differences between HMI and the urban and rural sites
253 are analyzed in more detail in the companion paper (Balasus et al., 2021). In the companion
254 paper, episodic NH_3 events that derived from dairy, poultry, and industrial sources were
255 characterized (Balasus et al., 2021). For the events with complete aerosol composition and
256 meteorology data (8 out of 11 NH_3 events total), the average and median aerosol pH values (2.00
257 and 1.96, respectively) were only moderately higher than the study average and median pH



258 values (1.85 and 1.83, respectively); this difference is not statistically significant at the 95%
259 confidence interval. This includes an aerosol pH of 1.92 at the peak NH_3 concentration observed
260 during the entire study ($19.3 \mu\text{g m}^{-3}$), an event influenced by industrial emissions near downtown
261 Baltimore (Balasus et al., 2021). Together, the results suggest that pH may be more affected by
262 the proximity of the HMI site to the Chesapeake Bay than it was to regional agricultural NH_3
263 emissions, or to episodic NH_3 events from local industrial sources.

264

265 **3.3 Case Study: Effect of NVCs on pH**

266 NVCs affect thermodynamic predictions of NH_3 partitioning and thus, pH (Guo et al.,
267 2018; Vasilakos et al., 2018). Seawater is alkaline and primary marine emissions contain high
268 concentrations of NVCs (O'Dowd and De Leeuw, 2007). Marine aerosols rapidly acidify,
269 typically in seconds or minutes, though the timescale depends upon particle size (Angle et al.,
270 2021; Pszenny et al., 2004). Studies have examined the acidity of sea spray aerosols and their
271 evolution but none, to the authors' knowledge, have done so in a polluted urban environment.
272 The OWLETS-2 study offered a unique opportunity to analyze the pH of primary marine
273 particles emitted within several km of a large urban area. The Chesapeake Bay is brackish, with
274 increasing salinity moving down the bay towards the Atlantic Ocean (Pritchard, 1952). Near the
275 OWLETS-2 measurement site at HMI, salinity is variable but average conditions are $\sim 5 \text{ g kg}^{-1}$
276 (www.chesapeakebay.net, last accessed 20-November 2020). This is about a factor of seven
277 lower than typical seawater, but shows the potential for primary emissions to contribute salts that
278 could impact aerosol pH at HMI.

279 Elevated concentrations of Na^+ and Cl^- in $\text{PM}_{2.5}$ were infrequently observed during
280 OWLETS-2, with one notable 36-hour period showing evidence of primary marine impact. Na^+



281 and Cl^- were well-correlated ($R^2 = 0.78$) from 11-June to 13-June, a period that coincided with
282 the highest concentrations of both species (Fig. 6 and Fig. 7). It is noteworthy that wind speeds
283 were not elevated during this time (average winds = 3.1 m s^{-1} compared to campaign-average
284 wind speeds of 2.9 m s^{-1}); longer-term measurements would be needed to characterize factors
285 driving the primary bay emissions. During this event, the pH calculation using NH_3 partitioning
286 suggests that the primary marine emissions had a minimal effect on aerosol pH. The average pH
287 during this period was 1.98, which was only slightly higher than the average for the entire study
288 (1.85). Further, as the total $\text{Na}^+ + \text{Cl}^-$ concentration increased by more than an order of
289 magnitude, from $0.05 \mu\text{g m}^{-3}$ around 18:00 LT on 11 June to $0.9 \mu\text{g m}^{-3}$ at 09:00 LT on 12 June,
290 the pH only increased by 0.1 pH unit during the same period (Fig. 6). Gas-phase NH_3 data were
291 not available for the entire NaCl event, so pH calculations were limited to the first ~20 hours.

292 The pH predictions from ISORROPIA during this period display a more significant effect
293 on aerosol pH. The average pH predicted by ISORROPIA is 3.08, which is 0.7 pH units higher
294 than the study average from ISORROPIA. Further, while the pH calculated using NH_3
295 partitioning is insensitive to Na^+ and Cl^- , ISORROPIA predicts a rise of 1.4 pH units as Na^+ and
296 Cl^- increase (Figure 6). The NH_3 partitioning predicted by ISORROPIA deviates from the
297 observations during this event ($r = -0.19$, Fig. S7). The most likely explanation for this behavior
298 is different chemical compositions of the coarse- and fine-mode particles. Fresh marine
299 emissions acidify quickly, and evidence was found for chemical processing of NaCl. HNO_3
300 displacement of HCl is a well-known phenomenon in sea salt particles (Brimblecombe and
301 Clegg, 1988). Chloride:sodium ratios slightly above unity were observed when aerosol nitrate
302 concentrations were low, and below unity when nitrate concentrations were elevated (Fig. 7).
303 Nitrate formation, including HNO_3 uptake to sea salt, is highly sensitive to pH (Kakavas et al.,



2021; Vasilakos et al., 2018). Nitrate (along with Na^+ and Cl^-) are direct inputs to ISORROPIA, suggesting that the pH trend in Fig. 6 is due to the increased influence of coarse-mode particles. The PILS inlet was equipped with a $2.5\ \mu\text{m}$ cut-point cyclone (URG-2000-30-EH, URG Corp.), which allows some penetration of particles with $d_p < 4.5\ \mu\text{m}$ (<http://www.urgcorp.com/products/inlets/teflon-coated-aluminum-cyclones/urg-2000-30eh>, last accessed 29 January 2021). Likewise, primary sea salt emissions often exhibit a size distribution tail that extends below $2.5\ \mu\text{m}$ (Feng et al., 2017).

The above analysis identifies limitations computing aerosol pH with both approaches and highlights opportunities to use complementary information from each to inform factors driving aerosol pH. ISORROPIA's assumption of an internally mixed aerosol distribution cannot be applied to predict pH in this system (Fountoukis and Nenes, 2007). However, it does provide insight into the likely presence of coarse mode particles with pH significantly higher than the fine mode. Conversely, Na^+ , Cl^- and NO_3^- are not direct inputs into the pH calculation using NH_3 partitioning, though they are used to compute aerosol liquid water, which is an input in the pH calculation (Zheng et al., 2020). These NVCs have been shown to have sometimes significant effects on the ratios of ammonium-sulfate, which could lead to inconsistencies in the calculation of aerosol pH when considered in the ALWC calculation only (Guo et al. 2015). NH_4^+ resides predominantly in the fine mode (Seinfeld and Pandis, 2016), so the partitioning approach is unlikely to capture the acidity of the coarse mode or fine-mode particles in the tail of the distribution of primary emissions that may be externally mixed with secondary particles, such as dust or sea salt. This may lead to underestimates of NVC effects on aerosol pH using the partitioning approach. The combined information from both methods suggests that aerosols sampled at HMI during the NaCl event were characterized by a strong size-dependent pH



327 gradient, with fine-mode particles more acidic (pH ~2) than the coarse mode (pH up to 4.5).
328 Estimates of pH derived from size-segregated aerosol composition measurements have observed
329 the same phenomenon (Angle et al., 2021; Fang et al., 2017; Kakavas et al., 2021; Keene et al.,
330 2002).

331

332 **4 Conclusions**

333 There is growing recognition of the importance of aerosol pH affecting atmospheric
334 processes relevant to public health and ecosystems (Fang et al., 2017; Nenes et al., 2021).
335 Observations of spatial and temporal variations in pH are needed so that the factors that control
336 pH and contribute to variability in different environments can be fully understood. This study is
337 unique as it represents the first characterization of aerosol pH at a land-water transition site near
338 a large urban area. Baltimore, MD, is impacted by regional agricultural emissions and by
339 industrial point-source emissions of NH₃. The companion paper examines the sources of
340 episodic NH₃ events and the associated effects on aerosol composition (Balasus et al., 2021).
341 Although average and peak NH₃ concentrations during this study were significantly higher than a
342 nearby inland site, the effects on aerosol pH appear relatively insignificant, as pH during the
343 peak events was only ~0.1 pH unit higher than non-event periods. This finding is consistent with
344 studies at other locations that show aerosol pH is often insensitive to Tot-NH₃ and to the aerosol
345 NH₄:SO₄ ratio (Weber et al., 2016; Zheng et al., 2020; Tao and Murphy, 2019).

346 The unique characteristics of the OWLETS-2 study and measurement locations also
347 offered insight into the composition and meteorological influences on aerosol pH. In the
348 companion paper, the composition effects were shown to be muted in comparison to the
349 meteorological effects (Balasus et al., 2021). It was shown that the unique diurnal profiles,



350 particularly in ALW (which did not correlate with RH) and ε_{NH_3} (which did not correlate with T)
351 resulted in meteorological factors, notably temperature, having the most important influence on
352 aerosol pH. Across the full temperature range of the study, the observed pH sensitivity to
353 temperature was -0.047 K^{-1} , with increases in sensitivity up to -0.085 K^{-1} when the temperature
354 was $> 293 \text{ K}$. The sensitivity of aerosol pH shown here is in good agreement with previous
355 studies in the Baltimore region and beyond, *e.g.* Toronto (Tao and Murphy, 2019; Battaglia et al.
356 2017). Conversely, aerosol pH was not strongly affected by ALWC during the OWLETS-2
357 study, except when ALWC was below $1 \mu\text{g m}^{-3}$, in contrast to the results of Zheng et al. (2020).
358 These results of Zheng et al. (2020) in identifying ALW as the most important factor driving
359 aerosol pH variability were derived from the results of studies in multiple locations, including
360 bulk aqueous solution. However, the analysis suggests that the factors that drive aerosol pH
361 variability may exhibit important site-to-site differences that must be considered before
362 generalizations are applied.

363 A case study of the NVC effect on aerosol pH had significantly different outcomes
364 depending on the method for calculating pH. ISORROPIA predicted a pH increase of ~ 1.4 pH
365 units during an event with primary aerosol emissions from the Chesapeake Bay, while the pH
366 calculation using NH_3 partitioning predicted a much less significant effect (~ 0.1 pH unit). This
367 difference is attributed to the likely presence of externally mixed particles during the events,
368 which may include primary marine emissions elevated in NVCs. Bougiatioti et al. (2016)
369 evaluated aerosol pH at a remote site in the Mediterranean, where samples with a marine origin
370 demonstrated vastly different pH between fine (avg. pH = 0.4) and coarse mode (average pH =
371 7.3) particles. Similarly, Keene et al. (2002) demonstrated the effect of marine aerosol size
372 distribution on aerosol pH, with fine mode particles predicted to reside in the range of 1-2, with



373 super- μm particles to reside in the range of 3-4, consistent with the current results. Hence, a
374 limitation of this study is the lack of size-resolved aerosol composition measurements. This
375 study underscores the need to evaluate assumptions of internally mixed aerosols when applying
376 pH calculations, which may be a critical factor in overestimating the effects of NVCs on pH.
377 Models with size-resolved aerosol composition may be required to capture this effect across
378 scales in future studies (Kakavas et al., 2021).

379

380 **Data Availability**

381 Data are available at <https://www-air.larc.nasa.gov/cgi-bin/ArcView/owlets.2018>.

382

383 **Supplement**

384 **The supplement related to this article is available online at:**

385

386 **Acknowledgements**

387 A.G.C. and C.J.H. acknowledge funding from the National Science Foundation, AGS-1719252

388 and AGS-1719245. R.D. and V.C. acknowledge support by the National Oceanic and

389 Atmospheric Administration – Cooperative Science Center for Earth System Sciences and

390 Remote Sensing Technologies under the Cooperative Agreement Grant #: NA16SEC4810008.

391 N.B. and K.B. received support through the NOAA Office of Education, Educational Partnership

392 Program with Minority Serving Institutions (EPP/MSI).

393

394 **Author Contributions**



395 CH, AC, and RD conceived the analysis and study participation. MB, NB, and KB collected and
396 analyzed the PILS-IC and NH₃ data. NB, MB, and CH conducted the thermodynamic modeling
397 analyses. VC and AC provided analytical input and interpretation. NB, CH, KB, and MB wrote
398 the manuscript. All authors provided feedback and revisions to the manuscript.

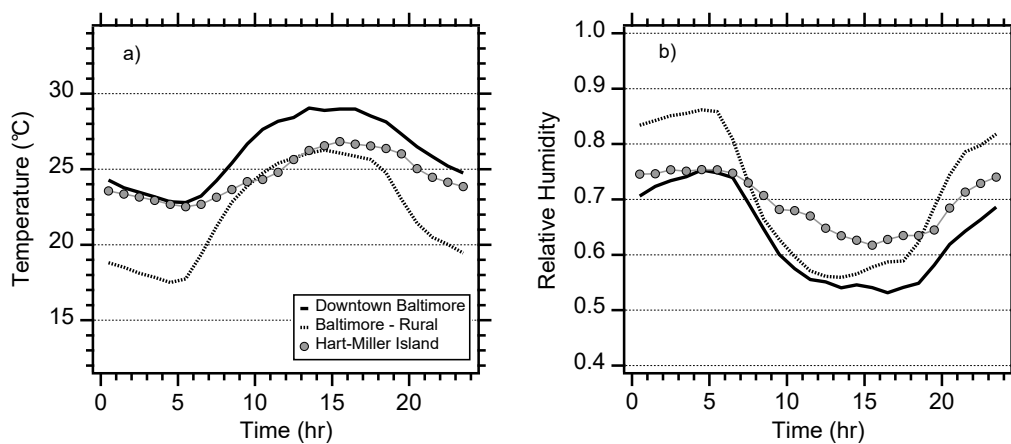
399

400 **Competing Interests**

401 The authors declare they have no conflict of interest.

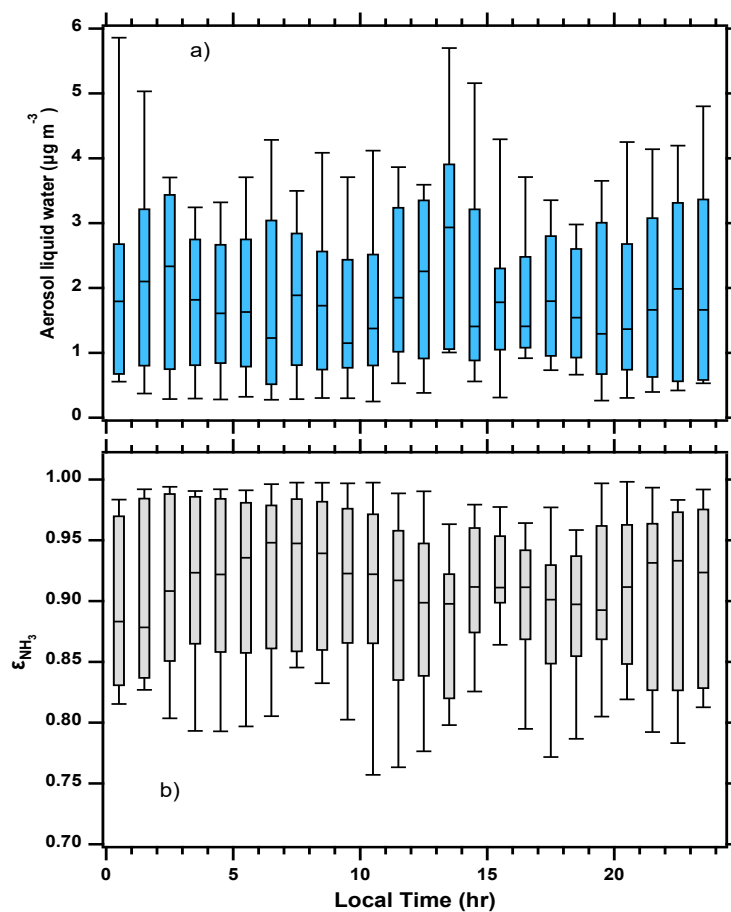


402 **Figures**
403



404

405 **Figure 1:** Diurnal profiles of (a) temperature and (b) relative humidity at three sites during the
406 OWLETS-2 study. Hart-Miller Island (HMI) is a land-water transition site and was the location
407 of aerosol composition and gas-phase measurements during the campaign. Temperatures at HMI
408 resembled the downtown location during the night but showed characteristics of the rural site
409 during the day. RH at HMI was between the urban and rural sites at night but was elevated
410 during the daytime due to the Chesapeake Bay.

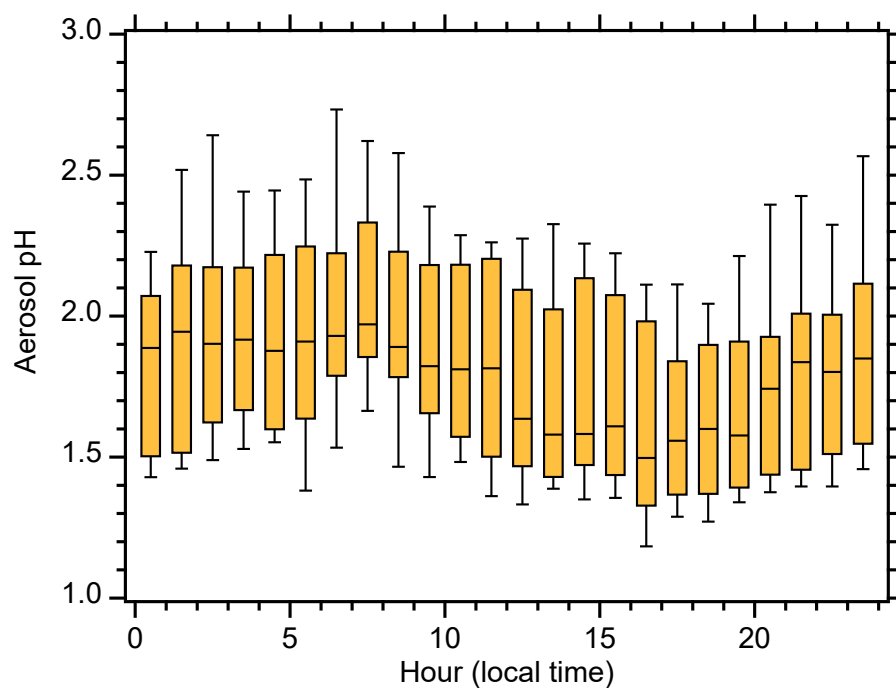


411

412 **Figure 2:** Box plots of (a) aerosol liquid water and (b) ϵ_{NH_3} ($\epsilon_{NH_3} = NH_3(g)/(NH_3(g) + NH_4^+(aq))$)

413 during the OWLETS-2 study. The statistics shown are the median, quartiles, 10th and 90th

414 percentiles.

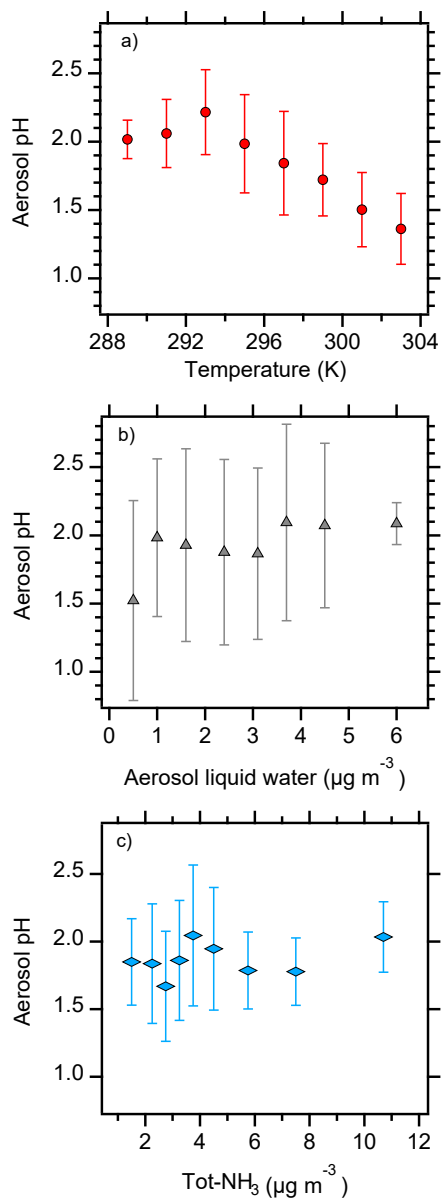


415

416 **Figure 3:** Box plot of the aerosol pH diurnal profile calculated using the method of Zheng et al.

417 (2020) at Hart-Miller Island during OWLETS-2. The statistics shown are the median, quartiles,

418 10th and 90th percentiles.

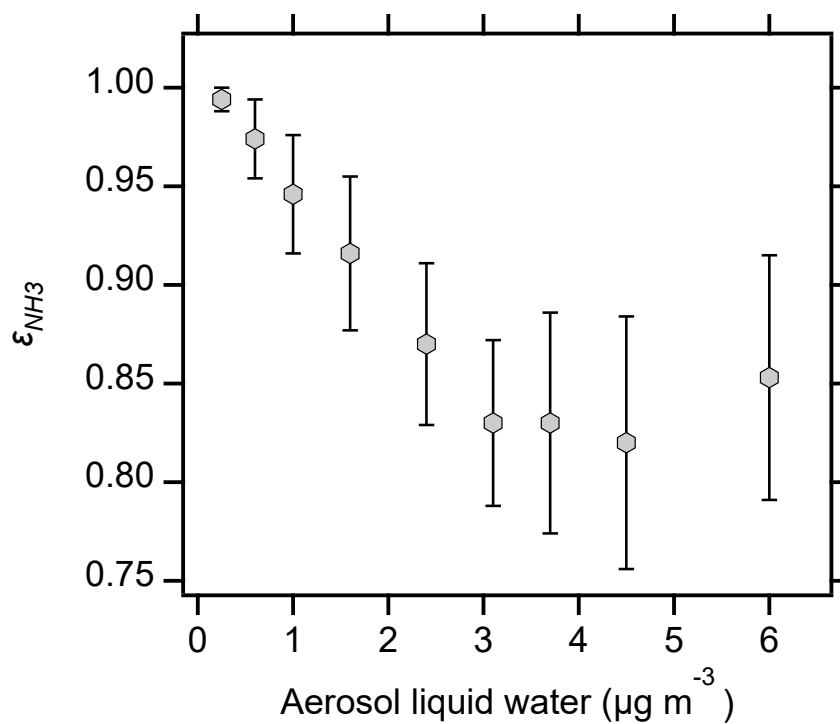


419

420 **Figure 4:** Relationship between aerosol pH and (a) temperature, (b) aerosol liquid water, and (c)

421 total NH₃ (Tot-NH₃ = NH₃ + NH₄⁺). Symbols represent mean values while error bars represent

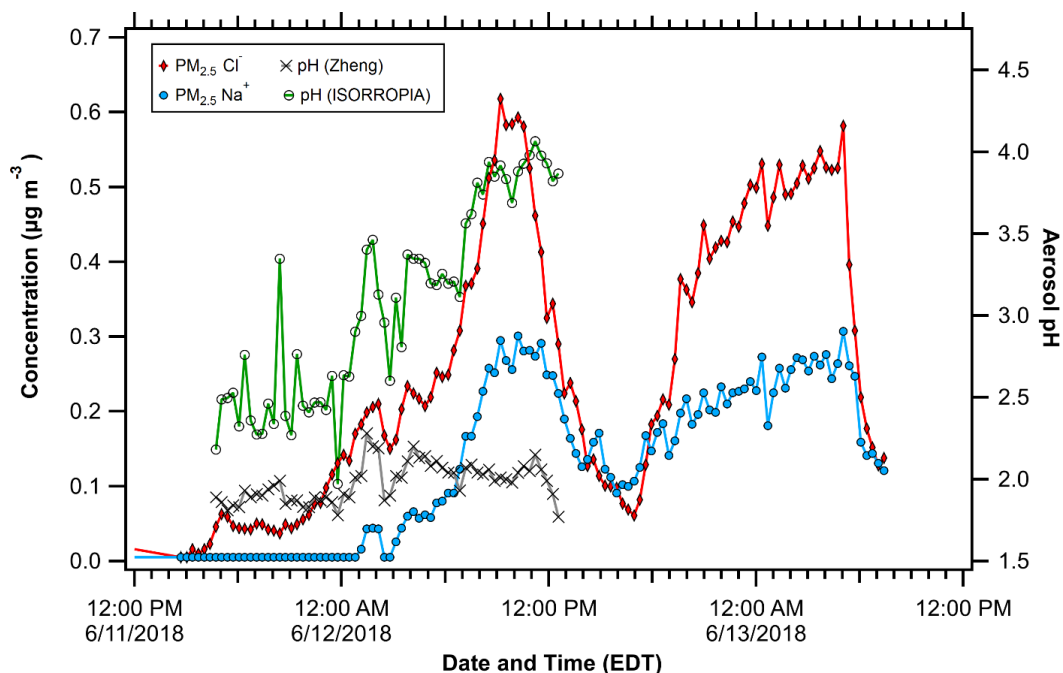
422 standard deviations.



423

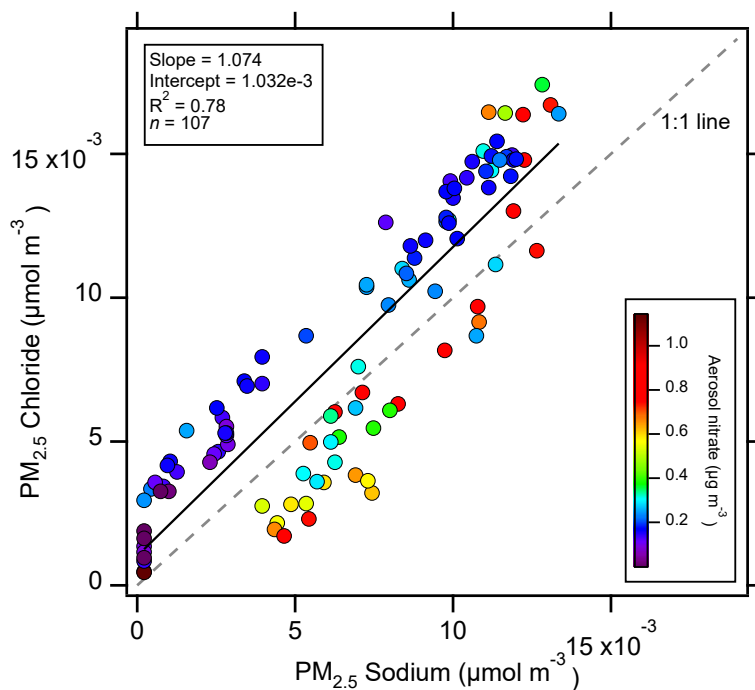
424 **Figure 5:** Relationship between NH_3 partitioning ($\epsilon_{\text{NH}_3} = \text{NH}_3/(\text{NH}_3 + \text{NH}_4^+)$) and aerosol liquid
425 water. Symbols represent mean values while error bars represent standard deviations.

426



427

428 **Figure 6:** Concentrations of $\text{PM}_{2.5} \text{Na}^+$ and Cl^- during a period with primary Chesapeake Bay
429 emissions. Aerosol pH calculated by NH_3 partitioning (Zheng et al. method) and ISORROPIA
430 show different behaviors, suggesting the aerosol distribution was externally mixed during this
431 time.



432

433 **Figure 7:** Correlation between $\text{PM}_{2.5} \text{Na}^+$ and Cl^- during the event shown in Figure 6. Lower
434 chloride:sodium ratios were observed at higher NO_3^- concentrations, suggesting HNO_3 uptake
435 displaced HCl .



436 **References**

437

438 Angle, K. J., Crocker, D. R., Simpson, R. M. C., Mayer, K. J., Garofalo, L. A., Moore, A. N., Garcia, S.
439 L. M., Or, V. W., Srinivasan, S., Farhan, M., Sauer, J. S., Lee, C., Pothier, M. A., Farmer, D. K.,
440 Martz, T. R., Bertram, T. H., Cappa, C. D., Prather, K. A., and Grassian, V. H. (2021). Acidity
441 across the interface from the ocean surface to sea spray aerosol. *Proceedings of the National
442 Academy of Sciences of the United States of America*, 118(2), Article e2018397118.
443 <https://doi.org/10.1073/pnas.2018397118>

444 Balasus, N., Battaglia, M. A., Ball, K., Caicedo, V., Delgado, R., Carlton, A.G., and Hennigan, C.J.
445 (2021). Urban aerosol chemistry at a land-water transition site during summer - part 1: impact of
446 agricultural and industrial ammonia emissions. *Atmos. Chem. Phys. Discussions*. In review.

447 Battaglia Jr, M. A., Weber, R. J., Nenes, A., and Hennigan, C. J. (2019). Effects of water-soluble organic
448 carbon on aerosol pH. *Atmos. Chem. Phys.*, 19(23), 14607-14620. [https://doi.org/10.5194/acp-19-
449 14607-2019](https://doi.org/10.5194/acp-19-14607-2019)

450 Battaglia, M. A., Douglas, S., and Hennigan, C. J. (2017). Effect of the Urban Heat Island on Aerosol pH.
451 *Environ. Sci. Technol.*, 51(22), 13095-13103. <https://doi.org/10.1021/acs.est.7b02786>

452 Bougiatioti, A., Nikolaou, P., Stavroulas, I., Kouvarakis, G., Weber, R., Nenes, A., Kanakidou, M., and
453 Mihalopoulos, N. (2016). Particle water and pH in the eastern Mediterranean: source variability
454 and implications for nutrient availability. *Atmos. Chem. Phys.*, 16(7), 4579-4591.
455 <https://doi.org/10.5194/acp-16-4579-2016>

456 Brimblecombe, P., and Clegg, S. L. (1988). The Solubility and Behavior of Acid Gases in the Marine
457 Aerosol. *Journal of Atmospheric Chemistry*, 7(1), 1-18. <https://doi.org/10.1007/bf00048251>

458 Carlton, A. M. G., Pye, H. O. T., Baker, K. R., and Hennigan, C. J. (2018). Additional benefits of federal
459 air quality rules: model estimates of controllable biogenic secondary organic aerosol.
460 *Environmental Science and Technology*. <https://doi.org/10.1021/acs.est.8b01869>

461 El-Sayed, M. M. H., Amenumey, D., and Hennigan, C. J. (2016). Drying-Induced Evaporation of
462 Secondary Organic Aerosol during Summer. *Environmental Science and Technology*, 50(7),
463 3626-3633. <https://doi.org/10.1021/acs.est.5b06002>

464 Fang, T., Guo, H. Y., Zeng, L. H., Verma, V., Nenes, A., and Weber, R. J. (2017). Highly Acidic
465 Ambient Particles, Soluble Metals, and Oxidative Potential: A Link between Sulfate and Aerosol
466 Toxicity. *Environmental Science and Technology*, 51(5), 2611-2620.
467 <https://doi.org/10.1021/acs.est.6b06151>

468 Feng, L., Shen, H., Zhu, Y., Gao, H., and Yao, X. (2017). Insight into Generation and Evolution of Sea-
469 Salt Aerosols from Field Measurements in Diversified Marine and Coastal Atmospheres.
470 *Scientific Reports*, 7, Article 41260. <https://doi.org/10.1038/srep41260>

471 Fountoukis, C., and Nenes, A. (2007). ISORROPIA II: a computationally efficient thermodynamic
472 equilibrium model for K^+ - Ca^{2+} - Mg^{2+} - NH_4^+ - Na^+ - SO_4^{2-} - NO_3^- - Cl^- - H_2O aerosols. *Atmos. Chem.
473 Phys.*, 7(17), 4639-4659. <https://doi.org/10.5194/acp-7-4639-2007>

474 Guo, H., Liu, J., Froyd, K. D., Roberts, J. M., Veres, P. R., Hayes, P. L., Jimenez, J. L., Nenes, A., and
475 Weber, R. J. (2017). Fine particle pH and gas-particle phase partitioning of inorganic species in



- 476 Pasadena, California, during the 2010 CalNex campaign. *Atmos. Chem. Phys.*, 17(9), 5703-5719.
477 <https://doi.org/10.5194/acp-17-5703-2017>
- 478 Guo, H., Nenes, A., and Weber, R. J. (2018). The underappreciated role of nonvolatile cations in aerosol
479 ammonium-sulfate molar ratios. *Atmos. Chem. Phys.*, 18(23), 17307-17323.
480 <https://doi.org/10.5194/acp-18-17307-2018>
- 481 Guo, H., Xu, L., Bougiatioti, A., Cerully, K. M., Capps, S. L., Hite, J. R., Carlton, A. G., Lee, S. H.,
482 Bergin, M. H., Ng, N. L., Nenes, A., and Weber, R. J. (2015). Fine-particle water and pH in the
483 southeastern United States. *Atmos. Chem. Phys.*, 15(9), 5211-5228. <https://doi.org/10.5194/acp-15-5211-2015>
484
- 485 He, H., Stehr, J. W., Hains, J. C., Krask, D. J., Doddridge, B. G., Vinnikov, K. Y., Canty, T. P., Hosley,
486 K. M., Salawitch, R. J., Worden, H. M., and Dickerson, R. R. (2013). Trends in emissions and
487 concentrations of air pollutants in the lower troposphere in the Baltimore/Washington airshed
488 from 1997 to 2011. *Atmospheric Chemistry and Physics*, 13(15), 7859-7874.
489 <https://doi.org/10.5194/acp-13-7859-2013>
- 490 Hennigan, C. J., Izumi, J., Sullivan, A. P., Weber, R. J., and Nenes, A. (2015). A critical evaluation of
491 proxy methods used to estimate the acidity of atmospheric particles. *Atmos. Chem. Phys.*, 15(5),
492 2775-2790. <https://doi.org/10.5194/acp-15-2775-2015>
- 493 Kakavas, S., Patoulias, D., Zakoura, M., Nenes, A., and Pandis, S. N. (2021). Size-resolved aerosol pH
494 over Europe during summer. *Atmos. Chem. Phys.*, 21(2), 799-811. <https://doi.org/10.5194/acp-21-799-2021>
495
- 496 Kanakidou, M., Myriokefalitakis, S., Daskalakis, N., Fanourgakis, G., Nenes, A., Baker, A. R., Tsigaridis,
497 K., and Mihalopoulos, N. (2016). Past, Present, and Future Atmospheric Nitrogen Deposition. *J.*
498 *Atmos. Sci.*, 73(5), 2039-2047. <https://doi.org/10.1175/jas-d-15-0278.1>
- 499 Keene, W. C., Pszenny, A. A. P., Maben, J. R., and Sander, R. (2002). Variation of marine aerosol acidity
500 with particle size. *Geophysical Research Letters*, 29(7), Article 1101.
501 <https://doi.org/10.1029/2001gl013881>
- 502 Keene, W. C., Pszenny, A. A. P., Maben, J. R., Stevenson, E., and Wall, A. (2004). Closure evaluation of
503 size-resolved aerosol pH in the New England coastal atmosphere during summer. *J. Geophys.*
504 *Res.-Atmos.*, 109(D23), D23307, Article D23307. <https://doi.org/10.1029/2004jd004801>
- 505 Loughner, C. P., Tzortziou, M., Follette-Cook, M., Pickering, K. E., Goldberg, D., Satam, C.,
506 Weinheimer, A., Crawford, J. H., Knapp, D. J., Montzka, D. D., Diskin, G. S., and Dickerson, R.
507 R. (2014). Impact of Bay-Breeze Circulations on Surface Air Quality and Boundary Layer
508 Export. *Journal of Applied Meteorology and Climatology*, 53(7), 1697-1713.
509 <https://doi.org/10.1175/jamc-d-13-0323.1>
- 510 Loughner, C. P., Tzortziou, M., Shroder, S., and Pickering, K. E. (2016). Enhanced dry deposition of
511 nitrogen pollution near coastlines: A case study covering the Chesapeake Bay estuary and
512 Atlantic Ocean coastline. *Journal of Geophysical Research-Atmospheres*, 121(23), 14221-14238.
513 <https://doi.org/10.1002/2016jd025571>



- 514 Nenes, A., Pandis, S. N., Kanakidou, M., Russell, A. G., Song, S., Vasilakos, P., and Weber, R. J. (2021).
515 Aerosol acidity and liquid water content regulate the dry deposition of inorganic reactive
516 nitrogen. *Atmos. Chem. Phys.*, 21(8), 6023-6033. <https://doi.org/10.5194/acp-21-6023-2021>
- 517 Nenes, A., Pandis, S. N., Weber, R. J., and Russell, A. (2020). Aerosol pH and liquid water content
518 determine when particulate matter is sensitive to ammonia and nitrate availability. *Atmos. Chem.*
519 *Phys.*, 20(5), 3249-3258. <https://doi.org/10.5194/acp-20-3249-2020>
- 520 Norman, M., Spirig, C., Wolff, V., Trebs, I., Flechard, C., Wisthaler, A., Schnitzhofer, R., Hansel, A., and
521 Neftel, A. (2009). Intercomparison of ammonia measurement techniques at an intensively
522 managed grassland site (Oensingen, Switzerland). *Atmospheric Chemistry and Physics*, 9(8),
523 2635-2645.
- 524 O'Dowd, C. D., and De Leeuw, G. (2007). Marine aerosol production: a review of the current knowledge.
525 *Philosophical Transactions of the Royal Society a-Mathematical Physical and Engineering*
526 *Sciences*, 365(1856), 1753-1774. <https://doi.org/10.1098/rsta.2007.2043>
- 527 Phillips, S. M., Bellcross, A. D., and Smith, G. D. (2017). Light Absorption by Brown Carbon in the
528 Southeastern United States is pH-dependent. *Environmental Science and Technology*.
529 <https://doi.org/10.1021/acs.est.7b01116>
- 530 Pinder, R. W., Adams, P. J., Pandis, S. N., and Gilliland, A. B. (2006). Temporally resolved ammonia
531 emission inventories: Current estimates, evaluation tools, and measurement needs. *Journal of*
532 *Geophysical Research-Atmospheres*, 111(D16), Article D16310.
533 <https://doi.org/10.1029/2005jd006603>
- 534 Pritchard, D. W. (1952). Salinity Distribution and Circulation in the Chesapeake Bay Estuarine System.
535 *Journal of Marine Research*, 11(2), 106-123.
- 536 Pszenny, A. A. P., Moldanov, J., Keene, W. C., Sander, R., Maben, J. R., Martinez, M., Crutzen, P. J.,
537 Perner, D., and Prinn, R. G. (2004). Halogen cycling and aerosol pH in the Hawaiian marine
538 boundary layer. *Atmospheric Chemistry and Physics*, 4, 147-168. <https://doi.org/10.5194/acp-4-147-2004>
- 540 Pye, H. O. T., Nenes, A., Alexander, B., Ault, A. P., Barth, M. C., Clegg, S. L., Collett Jr, J. L., Fahey, K.
541 M., Hennigan, C. J., Herrmann, H., Kanakidou, M., Kelly, J. T., Ku, I. T., McNeill, V. F.,
542 Riemer, N., Schaefer, T., Shi, G., Tilgner, A., Walker, J. T., Wang, T., Weber, R., Xing, J.,
543 Zaveri, R. A., and Zuend, A. (2020). The acidity of atmospheric particles and clouds. *Atmos.*
544 *Chem. Phys.*, 20(8), 4809-4888. <https://doi.org/10.5194/acp-20-4809-2020>
- 545 Pye, H. O. T., Zuend, A., Fry, J. L., Isaacman-VanWertz, G., Capps, S. L., Appel, K. W., Foroutan, H.,
546 Xu, L., Ng, N. L., and Goldstein, A. H. (2018). Coupling of organic and inorganic aerosol
547 systems and the effect on gas-particle partitioning in the southeastern US. *Atmos. Chem. Phys.*,
548 18(1), 357-370. <https://doi.org/10.5194/acp-18-357-2018>
- 549 Seinfeld, J. H., and Pandis, S. N. (2016). *Atmospheric chemistry and physics: from air pollution to*
550 *climate change* (3 ed.). John Wiley and Sons.
- 551 Tao, Y. (2020). *Identification of Major Factors Influencing Aerosol pH and the Quantitative Relationship*
552 *between pH and Ammonia Gas/Particle Partitioning* [Doctoral thesis, University of Toronto].
553 University of Toronto TSpace. <https://hdl.handle.net/1807/103788>



- 554 Tao, Y., and Murphy, J. G. (2019). The sensitivity of PM_{2.5} acidity to meteorological parameters and
555 chemical composition changes: 10-year records from six Canadian monitoring sites. *Atmos.*
556 *Chem. Phys.*, 19(14), 9309-9320. <https://doi.org/10.5194/acp-19-9309-2019>
- 557 Valerino, M. J., Johnson, J. J., Izumi, J., Orozco, D., Hoff, R. M., Delgado, R., and Hennigan, C. J.
558 (2017). Sources and composition of PM_{2.5} in the Colorado Front Range during the DISCOVER-
559 AQ study. *Journal of Geophysical Research-Atmospheres*, 122(1), 566-582.
560 <https://doi.org/10.1002/2016jd025830>
- 561 Vasilakos, P., Russell, A., Weber, R., and Nenes, A. (2018). Understanding nitrate formation in a world
562 with less sulfate. *Atmos. Chem. Phys.*, 18(17), 12765-12775. [https://doi.org/10.5194/acp-18-](https://doi.org/10.5194/acp-18-12765-2018)
563 [12765-2018](https://doi.org/10.5194/acp-18-12765-2018)
- 564 Weber, R. J., Guo, H., Russell, A. G., and Nenes, A. (2016). High aerosol acidity despite declining
565 atmospheric sulfate concentrations over the past 15 years [Letter]. *Nature Geoscience*, 9(4), 282-
566 285. <https://doi.org/10.1038/ngeo2665>
- 567 Zheng, G., Su, H., Wang, S., Andreae, M. O., Pöschl, U., and Cheng, Y. (2020). Multiphase buffer theory
568 explains contrasts in atmospheric aerosol acidity. *Science*, 369(6509), 1374.
569 <https://doi.org/10.1126/science.aba3719>